Modulated phases, magnetic phase diagrams, and the Lifshitz point in MnP from the mean field theory

Andrzej Zieba, Monika Slota, and Mariusz Kucharczyk
Department of Physics and Nuclear Techniques, University of Mining and Metallurgy, Al. Mickiewicza 30, 30-059 Kraków, Poland
(Received 7 May 1999)

The axial next-nearest-neighbor Heisenberg (ANNNH) model with orthorhombic magnetocrystalline anisotropy was applied to describe magnetic phases and phase transitions occurring in manganese phosphide in magnetic field **H** applied along the lattice vectors **a**, **b**, and **c**. The ground state of the Hamiltonian was obtained using analytical methods of Nagamiya's theory, augmented by numerical minimization of the energy with respect to the wave vector q of the modulated magnetic structures (heli, fan, cone). The latter procedure leads to the dependence $q(H)$ for all modulated phases, and explains both the shapes of the magnetization curves for these phases (convex for the fan and concave for the cone phase) and the weakly first-order nature of the cone-fan phase transition. The magnetic phase diagrams for the three principal directions of the applied field, $\mathbf{H}\|\mathbf{c}$, $\mathbf{H}\|\mathbf{b}$, and $\mathbf{H}\|\mathbf{a}$, are calculated under the assumption that the ratio of competing nearest-neighbor and next-nearest-neighbor interactions depends on the temperature. The characteristics of special points in the phase diagrams (Lifshitz points, triple point, critical end point, and terminations of critical lines) remain in a semiquantitative accordance with experiment. For the Lifshitz point the deviation from asymptotic scaling laws was analyzed by calculating the effective (fit-range-dependent) values for the crossover exponent ϕ, the wave vector exponent β_k, and magnetization discontinuity exponent β_m. The results provide an explanation of their experimental values.

I. INTRODUCTION

Incommensurate magnetic structures of the orthorhombic metallic compound MnP are among the most thoroughly studied. Manganese phosphide orders ferromagnetically at 293 K and below 47 K it transforms into a helimagnetic phase with spins rotating within the easy *bc* plane.[1,2] An applied magnetic field **H** induces incommensurate structures, of the fan and cone type (Fig. 1). The structure of the fan phase and its evolution with the magnitude of the magnetic field were investigated using neutron diffraction[3–7] whereas the existence of the cone phase, inferred from macroscopic measurements,[8] awaits direct experimental verification.

Mapping the fairly complex magnetic phase diagram for the external field parallel to the **b** orthorhombic lattice vector ($a>b>c$) has led to the discovery[9] of the Lifshitz multicritical point (LP) at the confluence of fan, ferromagnetic, and paramagnetic phases. Although the critical behavior characteristic of the proximity to a LP seems to occur for a few helimagnets with a long-wavelength modulation (e.g., Tb)[10], manganese phosphide in an external magnetic field remains the only magnetic system for which the true LP, i.e., with a wave vector q of the modulated (fan) phase going to zero, was found and several critical exponents determined.[7–9,11–17]

MnP exhibits other features, which are of interest for phase-transition physics. The fan-para transition is an example of a critical transition which can be traced down to absolute zero temperature. The transition between cone and fan phases induced by an external field parallel to the orthorhombic *a* axis is an uncommon example of a continuous (or only weakly discontinuous) phase transition between two ordered phases (Fig. 2). This makes possible the existence of a critical end point at the confluence of the cone, fan, and ferromagnetic phase.[18] Measurements made for $Mn_{0.9}Co_{0.1}P$, the disordered homologue of MnP, have shown intriguing novel features such as irreversible behavior in all modulated phases, additional phases between helimagnetic and fan structures,[19,16] and the inverse hysteresis of the cone-fan transition.[20] (Inverse hysteresis means that the transition field for the increasing field is lower than for decreasing field.)

These results were not adequately discussed in terms of microscopic spin models. In particular, the properties of the Lifshitz point were interpreted using the results of the renormalization group theory for a suitable Landau-Ginzburg-Wilson (LGW) Hamiltonian.[21,22] (The parameters for the universality class of this LP are $d=3$, $n=1$, and $m=1$ where d,n, and m denote spatial, order parameter, and wave vector dimensionalities.) However, this theory makes predictions for the asymptotic universal properties of the LP and delivers no information on the behavior of the system a finite distance away from the LP.

The objective of this work was to obtain the ground-state solution for a realistic spin model of MnP, aiming at calculating the mean-field-type characteristics of its magnetic-modulated phases and phase transitions. The mean field calculation should also help in recognizing the effects of critical fluctuations, the possible influence of the itineracy of Mn electrons,[5] and the effects introduced by the quenched disorder ($Mn_{1-x}Co_xP$).

Localized spin models with the competing nearest-neighbor and next-nearest-neighbor interactions remain the simplest and the most fruitful models for incommensurate structures.[22] For Ising spins this approach is exemplified by the axial next-nearest-neighbor Ising (ANNNI) model, well known because of its devil's-staircase behavior. Magnetic-modulated structures are more realistically described using a

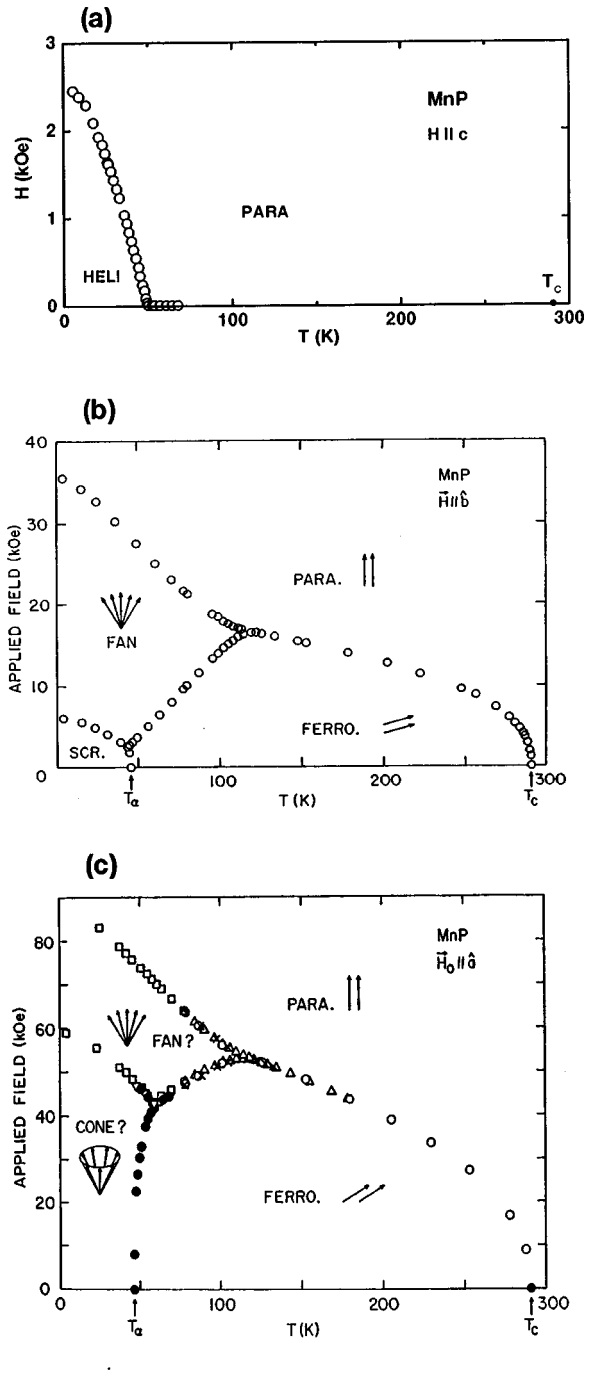

FIG. 1. Magnetic phase diagrams of MnP for a magnetic field parallel to three orthorhombic basic vectors: (a) **H**$\|$**c** (easy axis), replotted data of Huber and Ridgley (Ref. 1), (b) **H**$\|$**b** (intermediate axis), after Shapira *et al.* (Ref. 11), and (c) **H**$\|$**b** (hard axis), after Shapira *et al.* (Ref. 8).

Hamiltonian with the competing interactions between Heisenberg spins [axial next-nearest-neighbor Heisenberg (ANNNH) model] augmented with the magnetocrystalline anisotropy terms depending on the symmetry of the crystal lattice. The so-called Nagamiya's theory of incommensurate structures[23,24] is basically an analytical method for obtaining its ground state, i.e., the zero-temperature solution. Inomata and Oguchi[25] have adapted Nagamiya's theory to the case of orthorhombic anisotropy, and Hyamitzu and Nagamiya[26] have made quantitative calculations specific to MnP in external fields. The simple spin-wave theory of the origin of the heli-ferro transition in MnP was given by Smit[27] and the occurrence of the Lifshitz point at its magnetic phase diagrams was discussed by Yokoi, Countinho-Filho, and Salinas.[28] Models and solutions obtained in these works make the starting point for the present calculation.

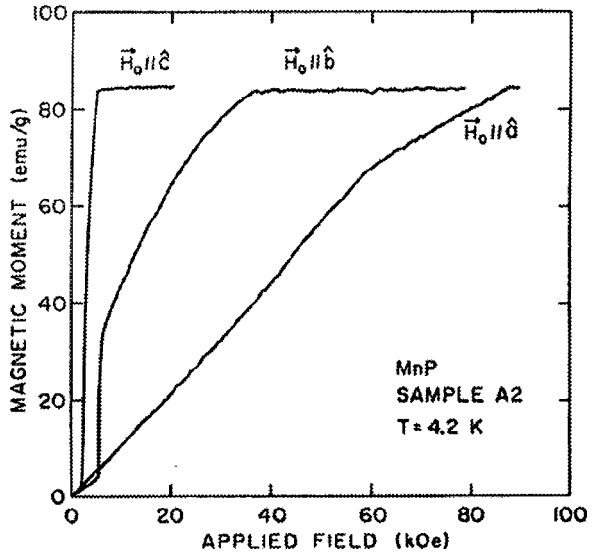

FIG. 2. Traces of the magnetization vs applied field at 4.2 K for fields applied parallel to the three principal crystallographic directions, after Ref. 8. For assigning different phases to the respective segments of $M(H)$ curves inspect Fig. 1.

The model Hamiltonian, the method of its solution, and the choice of model parameters are described in Sec. II. The classical spin Hamiltonian of the ANNNH type comprises a minimal set of terms necessary to account for the observed magnetic phases of MnP. One introduces the competing nearest-neighbor and next-nearest-neighbor interactions (J_1 and J_2, respectively) acting betweens layers of spins. The magnetocrystalline anisotropy is described using a lowest-order terms, with two anisotropy constants (K and K^z) required for the orthorhombic crystal symmetry. The number of model parameters is really smaller because the results depend, as usual for the ANNN-like models, on the competition ratio $\kappa = J_2/J_1$, and only one of two anisotropy constants is relevant as long as the magnetic field vector is confined to the *bc* plane.

To obtain the ground state of the Hamiltonian we followed approximate methods used in works of the Nagamiya group.[23–26] Energies of the trial spin structures were minimized analytically with respect to the modulation amplitudes. But in contrast to Hyamitzu and Nagamiya we performed the numerical *minimization of the energy with respect to the wave vector q*. This procedure allows one to calculate the dependence $q(H)$ in the modulated phases, and provides a much better approximation for their equilibrium energy. In addition to spin structures considered in the previous theoretical works[23–28] we made calculations for the *elliptical cone structure*, necessary to describe properly the phase transition between cone and fan phases and account for the existence of the critical end point.

The results of model calculations for three directions of the magnetic field (**H**$\|$**b**, **H**$\|$**c**, and **H**$\|$**a**) are presented and

discussed in relation to experiment in Secs. III and IV. Calculated magnetization curves and phase diagrams reveal features which are qualitatively novel with respect to those obtained for $q(H)=\text{const}$. Magnetic phase diagrams calculated as functions of $\kappa=J_2/J_1$ are related to the experimental H-T phase diagrams using an assumption that the competition ratio κ varies with the temperature.

Attention is paid (Sec. V) to the characteristics of the Lifshitz point occurring at $\mathbf{H}\|\mathbf{b}$ and $\mathbf{H}\|\mathbf{a}$ phase diagrams. The calculations allow one to derive three critical exponents and the amplitude ratios for the power law describing the phase boundaries. Close to the LP they must be the same as provided by the mean field solution of the LGW Hamiltonian for the uniaxial LP. The really interesting result is the calculation of the deviation from the power law where the distance from the LP is finite. This ''mean field correction to scaling'' is important to interpret the experimental exponents, necessarily derived from the data taken in finite ranges of temperature and magnetic field.

II. THEORETICAL MODEL AND METHOD OF ITS SOLUTION

A. Hamiltonian

The model considers equivalent N layers of spins S_n (with unit length), with the spins inside each layer coupled ferromagnetically. The directions of all the spins in the layer are assumed to be the same, and consequently the value of the in-plane coupling constant is irrelevant for the $T=0$ case. The exchange constants connecting the nth layer to the $(n+1)$st and $(n+2\text{nd})$ layers are J_1 and J_2, respectively.

The orthorhombic symmetry of the crystal lattice requires two second-order terms with anisotropy constants K and K^z. No higher-order terms are introduced. The first anisotropy constant (K) specifies the easy c axis and the intermediate b axis in the ''easy'' bc plane. The second one (K^z) is relevant when spins deviate from the bc plane. The energy of a given spin configuration (per one spin in a layer) is given by

$$E=-J_1\sum_{n=1}^{N}\mathbf{S}_n\cdot\mathbf{S}_{n+1}-J_2\sum_{n=1}^{N}\mathbf{S}_n\cdot\mathbf{S}_{n+2}+K\sum_{n=1}^{N}S_{x,n}^2+K^z\sum_{n=1}^{N}S_{z,n}^2-\mu\sum_{n=1}^{N}\mathbf{H}\cdot\mathbf{S}_n. \quad (1)$$

The orthorhombic lattice vectors **b**, **c**, and **a** correspond to the x,y, and z Cartesian coordinates.

B. Magnetic structures

The total energy of the system is a function of the magnetic structure. Minimization of the energy is done by the trial method, assuming a number of expected phases and comparing their equilibrium energies. Our analysis considers an external magnetic field **H** directed along the **c**, **b**, and **a** lattice vectors. The direction of spins in the nth layer (assumed the same) is specified by the polar angle θ_n measured from the a axis, and by the azimuthal angle ϕ_n measured from the c axis in the bc plane. In the following, the spin coordinates will be written, for simplicity, without the index n. Also we ignore the phase factor for trigonometric functions, irrelevant as long as modulated magnetic structures remain incommensurate with respect to the lattice.

The helimagnetic spin structure occurs in zero field and when it is within the easy plane. The direction of the nth spin is given by

$$\phi_n=nq+\xi_{q.}\sin nq+2\xi_{2q}\sin 2nq,\quad \theta_n=\frac{\pi}{2}. \quad (2)$$

In this equation the first term nq defines the regular helix. The second term with amplitude ξ_q accounts for the distortion of the helimagnetic structure due to an external magnetic field. (This term is responsible for its finite magnetization.) The third term describes the effect of the in-plane anisotropy, making the moments more crowded near the easy c axis. This distortion is known as the bunching effect: the amplitude ξ_{2q} is named the bunching parameter.[2]

The fan spin structure is stable for a nonzero applied field. The spins oscillate around the direction of the applied field within the plane for which the anisotropy energy is smaller. For a magnetic field parallel to the a axis the direction of moments is defined by

$$\sin\frac{\theta_n}{2}=\frac{\xi}{2}\cos nq. \quad (3)$$

The fan phase for other field directions ($\mathbf{H}\|\mathbf{b}$ and $\mathbf{H}\|\mathbf{c}$) can be defined in an analogous manner. The energy is calculated using a power expansion with respect to the modulation amplitude ξ. Hence the calculations are effectively performed using the following spin components:

$$S_z=1-\frac{1}{2}\xi^2\cos^2 nq,$$

$$S_y=\xi\cos nq-\frac{\xi^3}{8}\cos^3 nq. \quad (4)$$

This model of the fan phase phase, applied in Refs. 24–26, is not unique. Another model defined by the spin components ($S_y=\xi\sin nq$, $S_z=1-(\xi^2/2)\sin 2nq$) was introduced earlier by Nagamiya, Nagana, and Kitano (NNK).[23] For the fan structure defined by Eq. (4) it is the Zeeman term which is calculated exactly, whereas for the model of NNK the same concerns the anisotropy energy.

Two qualitatively different models of the cone phase, occurring for $\mathbf{H}\|\mathbf{a}$, are considered in this work. The circular cone is defined, after Hyamitzu and Nagamiya (HN),[26] as the distorted helimagnetic structure

$$\phi_n=nq+2\xi_{2q}\sin 2nq,\quad \theta_n=\text{const}. \quad (5)$$

The cone structure described by Eq. (5) transforms continuously, for $\theta_n\to\pi/2$, into the ''bunched'' helimagnetic structure. Its fundamental deficiency is that the circular cone cannot transform continuously into the fan structure.

The model of the *elliptical cone structure* introduced in this work,

$$S_x=\xi\sin nq-\frac{\zeta^3}{8}\sin^3 nq, \quad (6)$$

$$S_y=\xi\cos nq-\frac{\xi^3}{8}\cos^3 nq,$$

$$S_z=1-\frac{\xi^2}{2}\cos^2 nq-\frac{\xi^2}{2}\sin^2 nq-\frac{\xi^2\zeta^2}{4}\sin^2 nq\cos^2 nq,$$

describes mathematically the qualitative picture of the cone to fan transition given by Shapira *et al.*[8] The trial structure defined by Eq. (6) is a superposition of two fan modulations [Eq. (4)] shifted $\pi/2$ in phase. The cone-to-fan transition occurs when one of its amplitudes, namely, ζ, becomes zero. The mixed term ($\propto\xi^2\zeta^2$) in the S_z component is necessary to keep the unit length of the spin vector, up to the fourth-order powers of the modulation amplitudes ξ and ζ.

The elliptical cone phase, in analogy to the fan structure, can alternatively be described using the spin components $S_x=\xi\sin nq$, $S_y=\zeta\cos nq$, $S_z=1-(\xi^2/2)\sin^2 nq-(\zeta^2/2)\cos^2 nq$. This model, introduced by Nagamiya, Nagata, and Kitano,[23] can also account for the continuous nature of the fan-to-cone transition. We checked, however, that its quantitative predictions are numerically less accurate when compared to those obtained for the cone structure defined by Eq. (6). One reason is that for the model of NNK the relation $S_x^2+S_y^2+S_z^2=1$ is valid only up to the second powers of the modulation amplitudes.

In addition to the incommensurate structures described above we consider two commensurate magnetic phases, paramagnetic (P) and ferromagnetic (F). They are defined, respectively, as spin structures in which the magnetic moments are parallel to the applied field or make a constant angle with **H**.

C. Approximations

The energy and magnetization of the F and P phases are calculated exactly. In the absence of anisotropy and an external field, the wave vector of the helimagnetic structure is given by the well-known equation

$$\cos q_0=-\frac{1}{4\kappa}, \tag{7}$$

defining its ''ideal'' value q_0.

To describe the effect of anisotropy and external field the NNK's theory introduces approximations of two kinds. First, the modulated phases are defined using a finite number of parameters. These parameters are the wave vector q and modulation amplitudes ξ_q, ξ_{2q} for the helimagnetic, ξ for the fan, and ξ, ζ for the elliptical cone structure. Since the modulation of arbitrary shape can be described by the infinite Fourier series, a finite number of modulation amplitudes is equivalent to neglecting the higher-order Fourier terms.

The second approximation concerns the method of evaluating the energy for a given spin structure. The expansion of the spin components in a power series with respect to the modulation amplitudes makes it possible to calculate analytically the mean values for all terms appearing in the Hamiltonian [Eq. (1)] in the limit $N\to\infty$. The power series expansion is truncated at the fourth-order powers of modulation amplitudes. Dimensionless energy $e=E/(NJ_1)$ is thus given as a function of the wave vector q, the modulation amplitudes, and dimensionless parameters of the Hamiltonian: $\kappa=J_2/J_1$, $k=K/J_1$, $k^z=K^z/J_1$, and $h=\mu H/J_1$. For example, for the fan phase this expansion reads

$$e(\xi,q)=-\frac{j(0)}{2}+k-h+\frac{\xi^2}{4}[j(0)-j(q)-2k+h]+\frac{\xi^4}{64}[-2j(0)+3j(q)-j(2q)+6k]. \tag{8}$$

The ubiquitous quantity

$$j(mq)=2\cos mq+2\kappa\cos 2mq,\quad m=0,1,2,3, \tag{9}$$

represents the dimensionless Fourier transform coefficients of the exchange constants.

Since the energy is a quadratic form of the squares of modulation amplitudes, one can write down the formulas for the minimum energy in closed forms, which are functions of the wave vector q only. Explicit expressions for $e(q)$ for all phases are collected in the Appendix. Except for the elliptical cone these formulas are the same as those derived by HN,[26] but simplified by ignoring three additional Hamiltonian terms introduced in the HN work. The minimization of the energy $e(q)$ with respect to q is performed numerically.

The thus obtained equilibrium values of q are used to calculate magnetization curves. The formulas for $m(h)$ may be derived from Eqs. (A1)–(A8) as $m=-\partial e/\partial h$.

Quantitative inaccuracies resulting from both simplifying assumptions were checked (for the fan phase) by including an additional term in the Fourier transform and extending the calculation up to sixth order in the modulation amplitudes. Both options are analytically tractable; the formulas are given by HN [see Eqs. (2.12) and (C1)–(C5) in Ref. 26]. A numerical calculation shows that the change in the $m(h)$ and $q(h)$ curves is about 5%. Having in mind the simplified character of the Hamiltonian both approximations used in the calculations should be considered as reasonably accurate.

Two qualitative drawbacks of the method which was used should be mentioned. Formulas for the energies (A1)–(A6) are valid under the assumption that the period of the modulated phases is incommensurate. (This ensures a continuous distribution of the ϕ_n angles, making easy the calculation of the mean values of trigonometric functions.) A locking of the wave vectors into commensurate values (given by $q=2\pi P/Q$, where P,Q are integers) must occur for an exact solution of Hamiltonian (1) due to the effect of anisotropy and/or magnetic field. The recent study of Cadorin and Yokoi[29] for the ANNNXY model shows that the widths of commensurate heli and fan regions are becoming very narrow for long-period modulated structures. This probably explains the fact that there is no direct experimental evidence for a locking of the wave vector of fan or heli phases in MnP. Becerra, Oliveira, and Shapira[30] conjectured, however, that the observed behavior of the ac susceptibility of the fan phase may be understood as a result of jumps between innumerable commensurate phases.

Obviously any calculation for an *a priori* chosen set of trial structures excludes the possibility of discovering more exotic or unexpected modulated structures. The so-called he-

lifan and spin-flip structures were discovered via numerical minimization of the energy for a model with few hundred spin planes.[31]

D. Choice of model parameters for MnP

The orthorhombic structure of MnP may be viewed as a result of a distortion of a more symmetric hexagonal NiAs-type structure. For the NiAs-type structure the nearest-neighbor metal atoms belong to two equivalent planes. Similar ''layers'' of Mn atoms, with atom locations actually deviating somewhat off plane, occur for the MnP structure, and they correspond to the planes of spins in our model. Exchange constants J_1 and J_2 should be considered as *effective* interactions acting between nearest-neighbor and next-nearest-neighbor layers of spins. The real spin structure of the helimagnetic phase of MnP is of the double-helix type and it can be obtained as a ground state of the classical spin Hamiltonian with at least five isotropic exchange constants.[32]

Due to the presence of two layers of moments (spaced by $a/2$) for each lattice cell, the dimensionless wave vector q in model calculations corresponds to one-half of the experimental value (which is defined in relation to the a lattice constant). The experimental value of the modulation vector at low temperature (4.2 K) is $2q=0.117(2)$ (turn angle per layer, 21°). This corresponds, due to Eq. (7), to $\kappa=-0.268$. We assume that this low-temperature value of the competition ratio increases with temperature up to $\kappa=-1/4$ at the LP temperature.

Considering the MnP structure as a derivative of hexagonal ''parent'' structure is also useful in understanding its magnetocrystalline anisotropy. The orthorhombic **a** lattice vector, parallel to the former hexagonal axis, makes the hard axis of the magnetocrystalline anisotropy (characterized by the K^z anisotropy constant). The secondary effect of the orthorhombic distortion is to distinguish between the easy c and the intermediate b axes in the former hexagonal easy plane. This in-plane anisotropy is characterized by the K anisotropy constant ($K<K^z$).

If the in-plane anisotropy constant K were zero, the second-order heli-ferro transition in zero field would have occurred at $\kappa=-1/4$. The in-plane anisotropy extends the range of the ferromagnetic phase and makes the heli-ferro transition discontinuous. Experimentally this transition occurs at 47 K, at which temperature the turn angle of the helimagnetic phase decreases to 19°. Comparison of the equilibrium energies of helimagnetic [Eq. (A1)] and ferromagnetic [Eq. (A7)] phases for the corresponding wave vector $q=\pi\times 19°/180°$ allows us to determine the dimensionless in-plane anisotropy parameter $k=K/J_1=0.0032$.

The susceptibility of the ferromagnetic phase is inversely proportional to the anisotropy constant [Eq. (A8)]. The data of Huber and Rigley (Fig. 13 in Ref. 1) indicate that the anisotropy constant K^z is about 3 times larger than K. Hence we adopted a rounded value $k^z=0.01$.

The dimensionless magnetic field $h=\mu H/J_1$ is related to the real applied field, at least at low temperatures, by the ratio $H/h=320$ T. This last model parameter can be derived from the data (mentioned above) for the magnetic susceptibilities of the ferromagnetic phase.

The dimensionless results of the calculations do not depend on the absolute value of the exchange constant J_1. Nevertheless, one can estimate $J_1=24$ meV from the value of the H/h ratio given above and the experimental magnetic moment.

Our choice of model parameters κ and k follows the analysis of Smit.[27] The whole set can be compared to the Hamiltonian parameters obtained from the inelastic neutron scattering measurements on MnP by Tajima, Ishikawa, and Obara[33] and Yoshizawa, Shapiro, and Komatsubara.[34] The value $J_1=24$ meV falls between the estimates given in both papers.[35] The decrease of the $|J_2/J_1|$ ratio with the temperature is also confirmed. The combination of the anisotropy constants K and K^z can be related to the gap observed in the spin-wave spectrum.[34]

III. PROPERTIES OF THE MODULATED PHASES

A. Helimagnetic phase

Two limiting values of the modulation vector of heli phase in zero field were used to determine model parameters κ and k (Sec. II D). Nevertheless, one specific prediction can be obtained from the theory, namely, the amplitude of the bunching effect. The value of bunching parameter is given by the formula

$$\xi_{2q}=\frac{k}{j(q)-j(3q)}. \tag{10}$$

The calculated value $\xi_{2q}=0.013$ (for $\kappa=-0.268$) remains in rough agreement with the experimental value 0.0218 ± 0.0018, determined by Moon[2] using neutron diffraction. The discrepancy probably reflects the use of a one-sublattice model for the real double-helix structure.

As noted before, Eq. (7) defines the wave vector q_0 of the helimagnetic phase resulting from the sole interplay of competing exchange interactions. The magnetocrystalline anisotropy and magnetic field produce only a minor change of the wave vector (about 1%) with respect to this ''ideal'' value. This is because the change of q with respect to q_0 is proportional to the second powers of both k and h, $\cos q-\cos q_0 \propto h^2$, and $\cos q-\cos q_0 \propto k^2$. [A formula for $q(k)$ for the helimagnetic phase is given by Inomata and Oguchi. See Eq. (2.10) in Ref. 25.] The numerically calculated $q(h)$ in the helimagnetic phase, $\mathbf{H}\|\mathbf{b}$, is shown in Fig. 3.

B. Fan phase

The high-field paramagnetic phase becomes unstable with respect to fan modulation when the multiplicative coefficient in the ξ^2 term of the power expansion, Eq. (8), becomes negative. The function $j(q)$ [Eq. (9)] has a minimum at $q=q_0$. It follows from these two facts that the critical field of the second-order para-fan phase transition is given by

$$h_{FAN\text{-}P}=j(q_0)-j(0)+k, \tag{11}$$

and the wave vector equals q_0 at the transition field $h_{FAN\text{-}P}$. Equation (11) is written down for $\mathbf{H}\|\mathbf{b}$; for the field directions $\mathbf{H}\|\mathbf{c}$ and $\mathbf{H}\|\mathbf{a}$ the anisotropy parameter k in this equation should be replaced, respectively, by $-k$ and k^z.

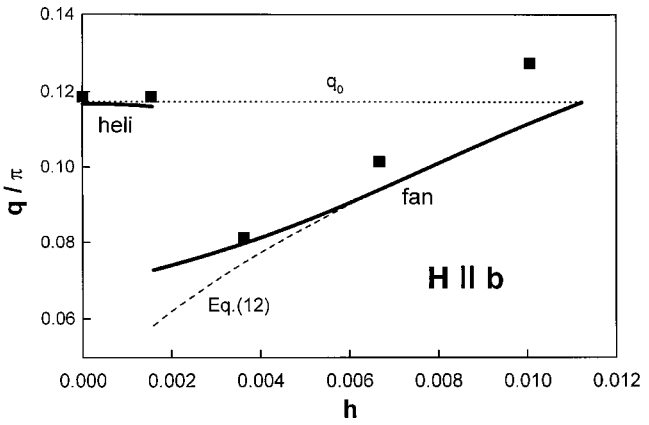

FIG. 3. The calculated and experimental dependence q/π vs h for helimagnetic and fan phases for $\mathbf{H}\|\mathbf{b}$, $\kappa=-0.268$. The solid line is calculated via numerical minimization of Eq. (A2), the dashed line represents Eq. (12), and the dotted line denotes the value q_0/π. Experimental points for 4.2 K are derived from Fig. 3 of Ref. 5.

On decreasing the field the wave vector decreases (Fig. 3). Besides the results obtained by numerical minimization of Eq. (A2) (Figs. 3 and 4), the dependence $q(h)$ for the fan phase can be calculated analytically for fields close to the transition field $h_{FAN\text{-}P}$. This was done first by NNK assuming zero in-plane anisotropy, i.e., for the pure ANNNXY model. [See Eq. (3.13) in Ref. 23.] Inomata and Oguchi[25] extended this calculation for the ANNNXY model with orthorhombic anisotropy. Their formula, after correcting a computational error,[36] and adapted for the $\mathbf{H}\|\mathbf{b}$ case, reads

$$\cos q=\cos q_0 + \frac{2\cos^2 q_0(1-\cos q_0)(1+2\cos q_0)}{(1+4\cos q_0+4\cos^2 q_0)(1-\cos q_0)^2+6k\cos q_0)} \times(h_{FAN\text{-}P}-h). \tag{12}$$

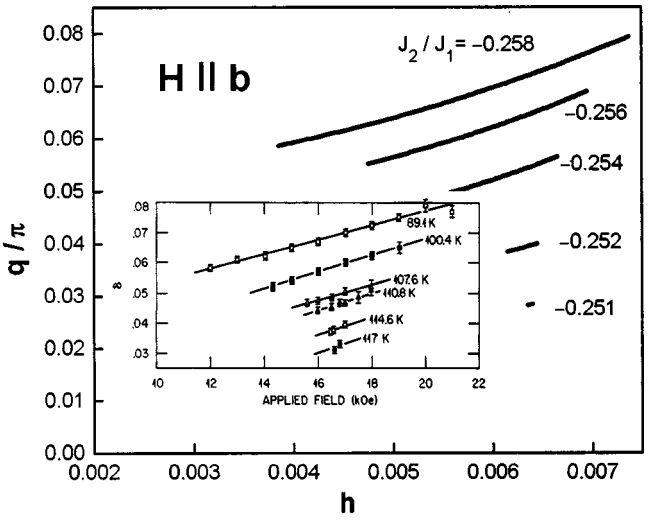

FIG. 4. Calculated q/p vs h for the indicated values of κ, $\mathbf{H}\|\mathbf{b}$. The inset shows the corresponding experimental data of Moon, Cable, and Shapira (Ref. 7).

The field dependence of the modulation vector of the fan phase is thus an inherent feature of localized spin models. The effect is strong when compared to a relatively weak $q(h)$ dependence for the helimagnetic phase because, as follows from Eq. (12), the change of q is linear in $(h_{FAN\text{-}P}-h)$. Another specific result of the theory is that the wave vector at the upper limit of the fan phase returns to its initial value ($\cong q_0$) in the helimagnetic phase in zero field.

It is surprising that these already existing theoretical results[23,25] for the localized spin model were never used to explain, even qualitatively, the strong $q(h)$ dependence in the fan phase of MnP, measured in several experimental works.[3–7] Obara *et al.*[5] have considered the field dependence of the modulation vector as an indication for the itinerant character of the magnetism of MnP. [They already found a correlation of the wave vector q with the extremal area of the Fermi surface deduced from de Haas–van Alphen (dHvA) effect.]

The numerically calculated $q(h)$ is compared in Fig. 3 to the approximate formula, Eq. (12), and to experimental results for 4.2 K. Calculation reproduces the approximately 30% decrease of the wave vector at the first-order heli-fan transition and its strong increase with field within the fan phase. The experimental wave vector rises at the upper limit of the fan phase above the value measured for the helimagnetic phase. Again, this probably reflects the deficiency of the one-sublattice model of the helimagnetic phase.

Standard analysis of Eq. (12) shows that the derivative dq/dh goes linearly to zero on approaching the Lifshitz point, i.e., for $\kappa=-1/4$. However, this limiting behavior shows up only very close to the LP. For experimentally relevant values of κ the calculated $q(h)$ curves are close to straight lines with the mean slopes only weakly dependent on the value of κ (Fig. 4). Both features are in agreement with the neutron diffraction data of Moon, Cable, and Shapira.[7] This experiment, performed for $89\leqslant T\leqslant 111$ K, shows the linear $q(H)$ dependence with the slope which seems almost independent of the temperature.

The calculated magnetization curve for $\kappa=-0.268$, Fig. 5, compares favorably to experimental one for $T=4.2$ K, shown in Fig. 2. For the fan phase calculation reproduces both an about 35% jump of the magnetization at the heli-fan transition and a decreasing slope of $m(h)$ on approaching the second-order fan-para transition. It should be stressed that this curvature is the outcome of using a field-dependent $q(h)$ to calculate $m(h)$. When the value of q is fixed, at q_0 or any other value, one necessarily obtains, within the approximations used, a linear $m(h)$ for all modulated phases. [See the calculated $m(h)$ curves in Ref. 26.]

The magnetization curves for $\kappa=-0.264$, -0.26, and -0.256 in Fig. 5 represent another sequence of phases, i.e., ferro-fan-para, occurring in MnP between 47 and 121 K. The slope of the $m(h)$ curve for the fan phase is clearly smaller than in the ferromagnetic phase and this fact accords with experimental results for the magnetization and ac susceptibility.[8,11] The only important feature which cannot be reproduced by the present mean-field-type calculation is the critical divergence of the susceptibility along the second-order fan-para and ferro-para phase boundaries.[13–15]

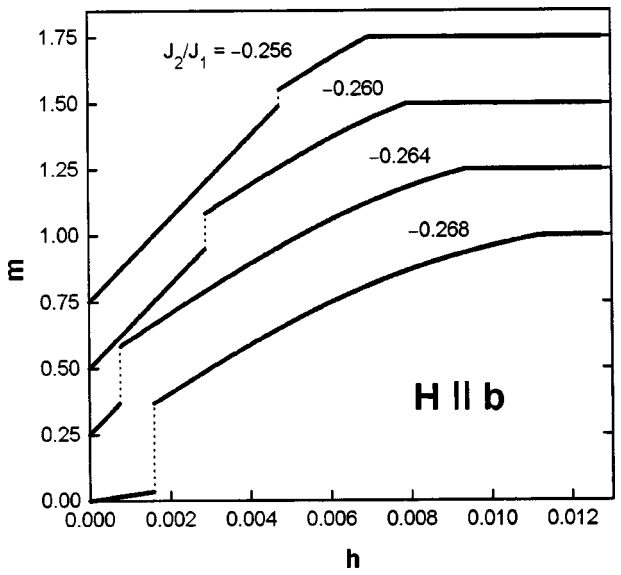

FIG. 5. Selected magnetization curves for $\mathbf{H}\|\mathbf{b}$, corresponding to the phase sequences heli→fan→para ($J_2/J_1=-0.268$) and ferro→fan→para ($J_2/J_1=-0.264$, -0.26, and -0.256). The subsequent $m(h)$ curves are, for clarity, vertically shifted.

C. Spin structure of the cone phase and the cone-fan transition

An analysis of the power expansion for the energy of an elliptical cone structure [Eq. (A3)] shows that the fan phase ($\xi^2>0$, $\zeta^2=0$) becomes unstable with respect to the formation of the cone phase ($\xi^2>0$, $\zeta^2>0$) at the transition field given by the equation

$$b_2-\frac{db_1}{2a_1}=0, \tag{13}$$

in which the symbols used denote the field-dependent coefficients [Eq. (A4)] in formula (A3) for the energy of the elliptical cone structure. This condition for the cone-fan transition was first derived, for a different model of the elliptical cone, by NNK. (See ''note added in proof'' in Ref. 23.) If the q value was fixed at q_0, the fan-cone transition would have been of the second-order type.

An unexpected outcome of the numerical minimization of the energy with respect to q is that the energy versus wave vector dependence may have two local minima: hence this transition may be first order. This occurs for the low-temperature value $\kappa=-0.268$. The discontinuities in the field dependence of the wave vector and in the magnetization curve are shown, respectively, in Fig. 6 and Fig. 7. The jump of magnetization amounts to 0.4% (at the equilibrium transition field) and the calculated hysteresis width is merely 0.12% of the transition field: hence the transition may be labeled as weakly first order. The evolution of the cone-fan transition into a continuous one, with the κ value tending to $-1/4$, will be discussed in Sec. IV.

The fact that the calculated $m(h)$ becomes negative for $h\to 0$ (inspect Fig. 7) is an artifact of the adopted trial structure for the elliptical cone. The circular cone model provides results which are numerically better in small and zero fields. The functions $q(h)$ and $m(h)$ calculated using the latter trial structure are shown in Figs. 6 and 7 using a dotted line. The exact ground state of the Hamiltonian would gently interpolate between these two limiting approximations.

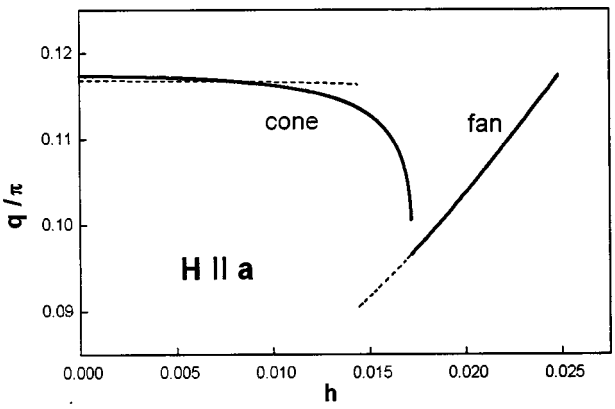

FIG. 6. Calculated dependence of the wave vector vs magnetic field for the cone and fan phases ($\mathbf{H}\|\mathbf{a}$, $J_2/J_1=-0.268$). Solid and dotted lines correspond to the elliptical cone and circular cone trial structures, respectively.

The calculated magnetization curve compares favorably with experiment (Fig. 2). It can explain the upward curvature of the $m(h)$ curve for the cone phase and its mean slope, about 2 times larger than that of the fan phase. The ratio of transition fields $h_{FAN\text{-}P}/h_{CONE\text{-}FAN}$ is also reproduced. Within the experimental resolution one cannot resolve the transition hysteresis or see the jump in the $m(h)$ curve. The weakly-first-order nature of the cone-fan transition is in line with conclusion of Shapira *et al.*[8] who describe it as ''either second order or very weakly first order'' below 15 K.

It will be interesting to investigate the evolution of the cone structure with field using neutron diffraction or other microscopic experimental techniques. The necessary magnetic field is within the reach of the actually available superconducting magnets. Such an experiment requires a careful alignment[8] of the single-crystal sample.

The results of model calculations may provide a hint at the explanation of the phenomenon of the cone-fan transition

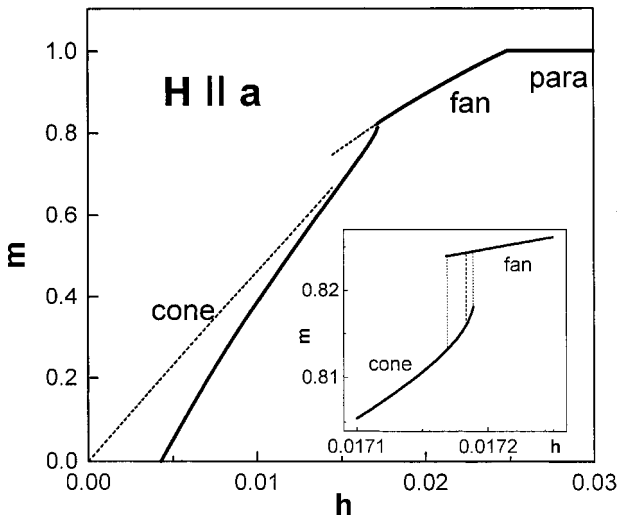

FIG. 7. Calculated magnetization curve for $\mathbf{H}\|\mathbf{a}$, $J_2/J_1=-0.268$, showing the phase sequence elliptical cone→fan→para. The dotted line shows $m(h)$ calculated for the circular cone structure. The inset shows a zoom-in at the weakly-first-order transition.

inverse hysteresis observed in $Mn_{0.9}Co_{0.1}P$. The experiment shows that for increasing field this transition occurs at a field value lower than the reverse transition for a decreasing field. [The hysteresis width is above 2% at 21 K and decreases to 0.5% at 30 K (Ref. 20 and 37).] Obviously, inverse hysteresis cannot occur when the considered phases remain in a thermodynamic equilibrium. It can be understood assuming that, due to some kind of pinning mechanism and the flatness of the $e(q)$ dependence for the cone phase, the wave vector q cannot evolve freely with the change of field. The calculation shows that the transition from the elliptical cone phase with q fixed into the fan phase in which q can freely relax should take place in a field which is smaller than that for the corresponding equilibrium transition. The very idea of a pinning of the wave vector in modulated phases of $Mn_{0.9}Co_{0.1}P$ is supported by observations of Fjellvag and Kjekshus[6] that the q value of its helimagnetic phase in a zero field does not change with the temperature.

IV. MAGNETIC PHASE DIAGRAMS FOR H ALONG THE ORTHORHOMBIC AXES

Results obtained for $\kappa=-0.268$ were discussed most thoroughly because they correspond to experimental results for 4.2 K, which is obviously a good approximation for the ground-state solution.

Our calculations do not contain explicitly the effect of finite temperature. The zero-temperature theory presented may be extended to finite temperatures assuming that the model parameters are temperature dependent. A change of effective exchange constants (and corresponding variation of the wave vector) should occur because of the spin-wave excitations.[27,38]

Smit[27] argues that the effect of spin waves produces a decrease of the effective J_2 and J_1 acting between the layers of spins, proportional to the decrease of their mean magnetization. This decrease is more rapid for J_2, thus producing the necessary 7% change of the competition ratio κ in the temperature range from 0 K to the Lifshitz point. Other model parameters may also be temperature dependent but the variation of κ is the most decisive and it ''generates'' the phase diagrams because κ is close to the critical value $-1/4$ and its small change brings about a large variation of the exchange energy.[27] Since the relation between the model parameters and temperature is only barely known, the phase diagrams were calculated [Figs. 8, 9(a), and 10] as functions of the dimensionless field h and the competition ratio κ, with the anisotropy parameters k and k^z kept fixed. The phase diagram for $\mathbf{H}\|\mathbf{b}$ shown in Fig. 9(b) is replotted in physical coordinates T and H using Eqs. (14) and (15) given below. Approximating the temperature decrease of the magnetization[39] by a classical ''3/2 law'' ($\Delta M/M \propto T^{3/2}$) one obtains from Smit's theory

$$\kappa(T)=\kappa(T=0)[1-c_\kappa T^{3/2}], \tag{14}$$

in which the coefficient c_κ was chosen to have $\kappa(T_L=121K)=-1/4$.

The relation between the real and effective fields is given in our model by $H=J_1 h/\mu$. The effective exchange constants are in Smit's theory proportional to the mean magnetization. Hence the ratio H/h decreases with increasing temperature and this decrease is approximated by

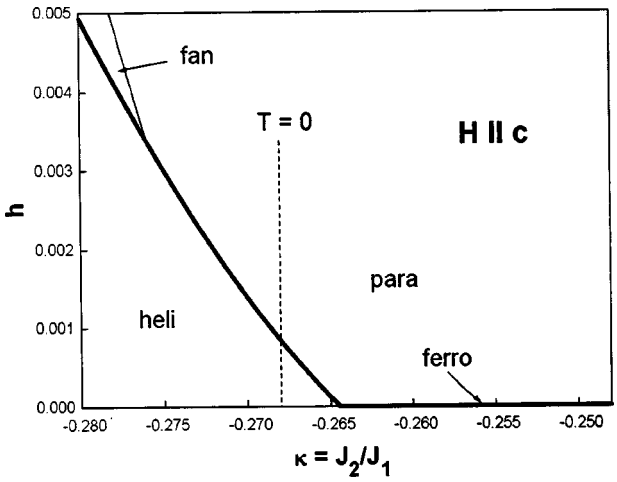

FIG. 8. Calculated magnetic phase diagram for $\mathbf{H}\|\mathbf{c}$. Thick and thin lines correspond to the first-order and the second-order transition lines, respectively.

$$\frac{H}{h}(T)=\frac{H}{h}(T=0)[1-c_m T^{3/2}]. \tag{15}$$

We adopted the value of c_m which gives the experimentally observed 10% decrease of the magnetization[39] at the LP temperature.

Comparison of the phase diagrams in Figs. 9(a) and 9(b) illustrates the relation between the h-κ and T-H phase diagrams for other directions of the applied field and shows the features which should appear in any theory describing correctly the effect of temperature. Equation (14) exemplifies the fact that the dependence $\kappa(T)$ should be nonlinear in order to have the slope dH/dT of all phase boundaries tending to zero at 0 K, as required by the third law of thermodynamics. On the high-temperature side of the phase diagram the decrease in the H/h ratio [Eq. (15)] gives rise to a downward bending of the ferro-fan phase boundary. (Calculation of the ferro-para phase boundary up to the Curie point is presented by Yoshizawa, Shapiro, and Komatsubara[34].)

The calculated phase diagram for $\mathbf{H}\|\mathbf{c}$ (Fig. 8) shows that only one modulated phase (helimagnetic) exists for the physically relevant range $\kappa>-0.268$. (The fan phase shows up for $\kappa<-0.276$.) The heli-para transition is discontinuous; for $\kappa=-0.268$ the magnetization jumps at this transition from $m=0.015$ to $m=1$. (Compare to Fig. 2.)

The most interesting feature of the phase diagram for $\mathbf{H}\|\mathbf{b}$ is the Lifshitz point and this issue is discussed in Sec. V. The phase boundaries at the junction of the heli-ferro-fan regions cross at sharp angles, as expected for the ordinary triple point. Perhaps the second most interesting special point (besides the LP) in this phase diagram is the termination of the critical phase boundary between the incommensurate fan phase and the paramagnetic phase at absolute zero of temperature. It should be interesting to determine experimentally the exponent in a presumably power law dependence $H_{FAN\text{-}P}(T)$ for $T\to 0$, in an analogy to similar investigations

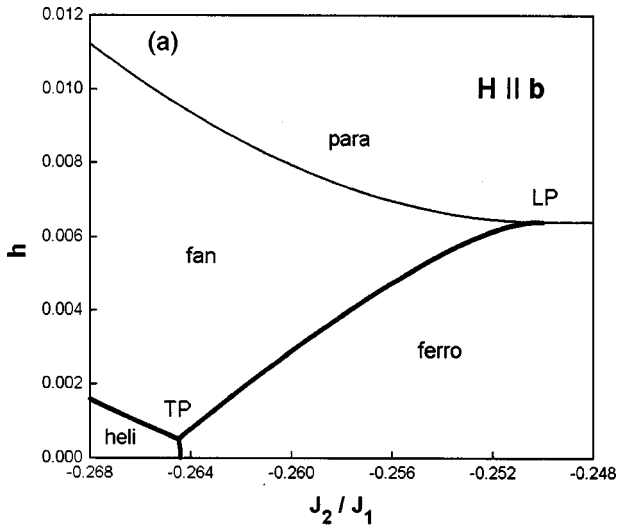

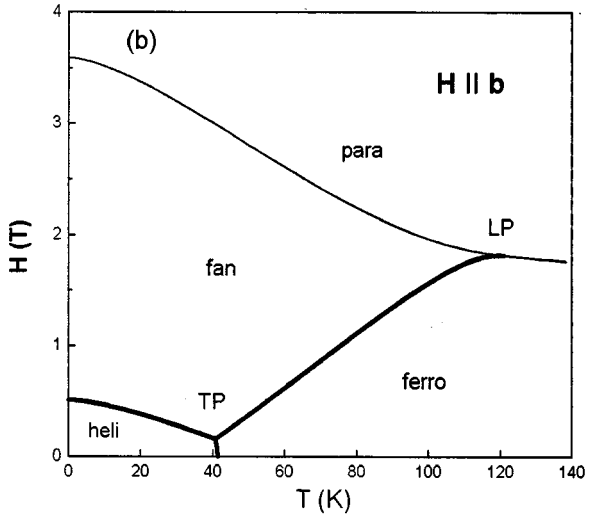

FIG. 9. Calculated magnetic phase diagram for **H**‖**b** using (a) $h-J_2/J_1$ coordinates and (b) H-T coordinates. Thick and thin lines are the first-order and the second-order phase boundaries, respectively. LP and TP denote the Lifshitz point and the triple point.

for commensurate antiferromagnets.[40,41] Assuming that the experimentally observed divergence of the ac susceptibility at the fan-para transition results from thermal critical fluctuations it should diminish on approaching 0 K.

The calculated phase diagram for **H**‖**a** is shown in Fig. 10. The cone-fan phase boundary, which is weakly first order for $\kappa=-0.268$ (as discussed in Sec. III C), changes into a continuous one at $\kappa=-0.2665$. As a result a tricritical point appears on the cone-fan phase boundary, and the cone-fan-ferro triple point is predicted to be the critical end point (CEP). The phase diagram exhibits the characteristic topology of the CEP, with the second-order line making a sharp angle with two mutually tangent first-order phase boundaries.

The behavior of the cone-ferro line in low field is an artifact of the elliptical cone model. The true solution of the Hamiltonian for $h\rightarrow 0$ should approach the phase boundary calculated for the circular cone (dotted line in Fig. 10).

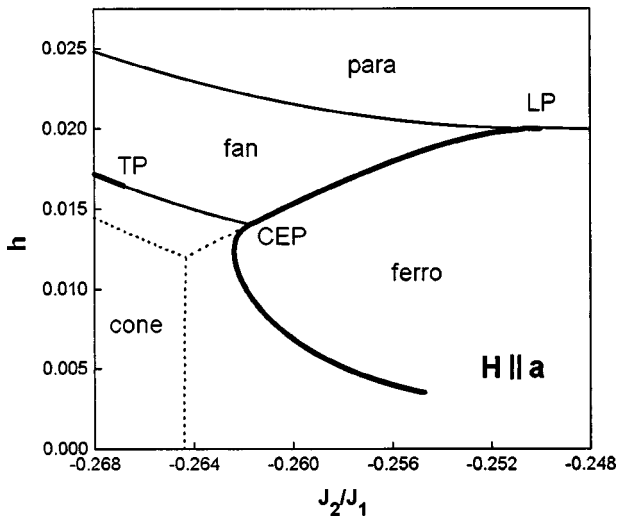

FIG. 10. Calculated magnetic phase diagram **H**‖**a**. Thick and thin solid lines show, respectively, the first-and the second-order transitions for the elliptical cone structure. LP, TCP, and CEP denote the Lifshitz point, the tricritical point, and the critical end point, respectively. Dotted lines show the change in the phase diagram when the elliptical cone is replaced by the circular cone trial structure. (CEP is then replaced by the triple point.)

How is this theory of the cone-fan transition related to the experiment? The overall phase diagram and in particular the shape of the cone-fan line and the first-order lines near the critical end point are in agreement with the experimental phase diagrams given in Refs. 8 and 18. Different opinions are presented in these papers on the character of the cone-fan transition. This transition is described by Shapira *et al.*[8] as ''either second order or very weakly first order'' below 15 K and ''weakly first order'' above this temperature. On the contrary Becerra *et al.*[18] found the cone-fan boundary to be continuous, at least for temperatures close to the CEP.

It is not easy to distinguish experimentally between the continuous (but close to first-order) and the weakly discontinuous transitions. The conclusion of Ref. 18 is in agreement with the present calculation. The authors of Ref. 8 suggest the possibility of a triple point at the cone-fan line, but, contrary to the present calculation, with the weakly-first-order transition at higher temperature. Both conclusions were derived from an analysis of the complex ac susceptibility data. The use of other experimental techniques is perhaps the best way to shed new light on the nature of the cone-fan transition in MnP.

All three calculated phase diagrams remain in remarkable agreement with experiment, especially when one recalls the fact that they were calculated using few model parameters extracted from the zero-field or the low-field data. The field and/or temperature coordinates of 11 (in total) special points are reproduced within some 20% accuracy. The exception is the factor of 2 discrepancy for the field of the heli-fan-fero triple point and the heli-fan transition field at $T=0$ (at **H**‖**b** phase diagram). The experimentally broader area of the helimagnetic phase may qualitatively be understood as a result of an additional lowering of its energy due to the formation of the double helix.

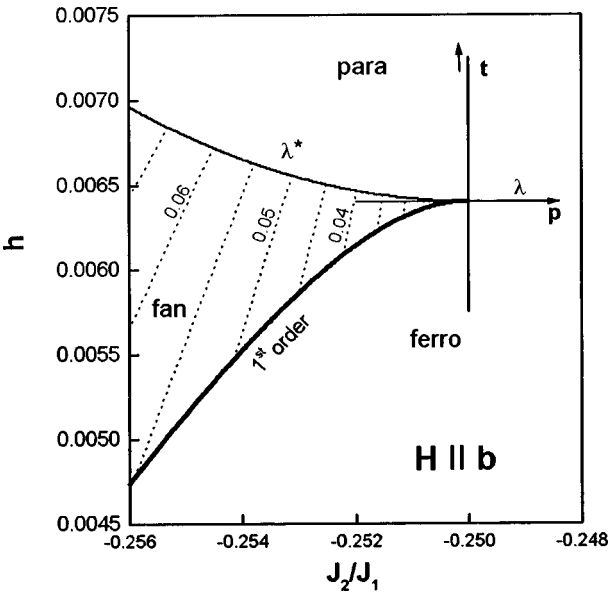

FIG. 11. The phase diagram for **H**∥**b** near the Lifshitz point. The *p* and *t* arrows denote asymptotic directions of the scaling axes. The lines of the constant wave vector (for the indicated values of q/π) are shown inside the domain of the fan phase.

V. LIFSHITZ POINT

A Lifshitz multicritical point occurs in the magnetic phase diagrams for **H**∥**b** and **H**∥**a**, at the confluence of ferro, fan, and para phases. In the mean field solution for the ANNNI, ANNNXY, and ANNNH Hamiltonians its location is solely determined by the ratio of exchange constants $\kappa=-1/4$. Assuming that the value of κ depends only on the temperature one can understand the fact that the temperature coordinate of the Lifshitz point is the same (121 K) for both field directions.[8]

For the isotropic ANNNH model the Lifshitz point occurs in zero field. It is the magnetocrystalline anisotropy which makes it possible for the Lifshitz point to occur at a nonzero magnetic field. The field coordinate of the LP for the model considered is proportional to the respective anisotropy constant, $h_L(\mathbf{H}\|\mathbf{b})=2k$, $h_L(\mathbf{H}\|\mathbf{a})=2k^z$.

A. Universal parameters for the Lifshitz point in MnP

A description of the critical behavior near the LP requires the use of two scaling variables. One of them (t) plays the role of temperature; the second one (p) determines the location of the LP at the critical line. Both are functions of physical fields (the magnetic field H and the temperature T). In a small vicinity of the LP the functions $p(H,T)$ and $t(H,T)$ can be linearized and under this assumption one may introduce a set of scaling axes p and t centered at the LP (Fig. 11).

The universal parameters of the Lifshitz point can be divided into two groups. The first comprises the exponents α_L, β_L, and γ_L and amplitude ratios defined in the usual manner for the measurement taken along the t axis, i.e., for $p=0$. For mean-field-theory- (MFT-) type models of the Lifshitz point these exponents have their usual mean field values.

The second group of the universal parameters, more specific to the LP, is related to power laws in which the p scaling variable is involved. We will discuss those exponents which can be derived from the model calculations. According to the extended scaling hypothesis the same crossover exponent ϕ describes the shape of three phase boundaries:

$$t_{FAN_P}=F_{\lambda *}p^{1/\phi}, \tag{16}$$

$$t_{F\text{-}FAN}=F_1 p^{1/\phi},$$

$$t_{F\text{-}P}=F_\lambda p^{1/\phi}.$$

Equations (16) imply that one can define two independent amplitude ratios for the phase boundaries, $F_\lambda/F_{\lambda *}$ and $F_1/F_{\lambda *}$. The subscripts indicate that they are related to two segments λ and λ^* of the critical line (Fig. 11) and to the first-order phase boundary, respectively.

The exponent β_k describes the behavior of the wave vector along the second-order phase boundary between paramagnetic and modulated phase,

$$q_{FAN\text{-}P}\propto p^{\beta_k}. \tag{17}$$

The exponent β_m is related to the discontinuity of the magnetization along the first-order phase boundary (ferro-fan),

$$\Delta m_{F\text{-}FAN}\propto p^{1/\beta_m}. \tag{18}$$

Mean field theories of the uniaxial Lifshitz point predict $\phi=1/2$, $\beta_k=1/2$, and $\beta_m=1/2$. The amplitude ratios for the phase boundaries are $F_1/F_{\lambda *}=2+\sqrt{6}=4.45$ and $F_\lambda/F_{\lambda *}=0$.

The experimentally determined exponents for MnP are summarized in Table I. To make use of Eqs. (16)–(18) one should relate the scaling variables p and t to the physical fields T and H. Since the crossover exponent $\phi<1$, the p axis (''hard'') is tangent to the phase boundaries, whereas the ''weak'' t axis cannot uniquely be determined from the shape of the phase diagram alone. It was assumed in all experimental works[7–9,11–17] that the t axis is vertical at the H-T phase diagram. Under this assumption the p scaling variable depends only on the temperature and can conveniently be defined as $p=(T_L-T)/T_L$. Thus one obtains the formula

$$H_{FAN\text{-}P}-H_{F\text{-}FAN}\propto p^{1/\phi}, \tag{19}$$

which makes it possible to determine the crossover exponent independently of the direction of the p axis and of the value of $F_1/F_{\lambda *}$ amplitude ratio.

The crossover exponent is the only one which was determined for different samples and field directions. However, because of use of Eq. (19), no value for the corresponding amplitude ratio $F_1/F_{\lambda *}$ is given in the literature. The experimental value for the second amplitude ratio $F_\lambda/F_{\lambda *}$ should be considered to be close to zero because the curvature of the ferro-para boundary near the LP is small (when compared to the fan-para line) and can be understood as resulting from the overall curvature of the ferro-para phase boundary.

The exponent β_m, related to the discontinuity of the magnetization along the first-order phase boundary, has only been measured for $Mn_{0.9}Co_{0.1}P$. Hysteresis is a nonequilibrium phenomenon and is not discussed in this work. Experi-

TABLE I. Universal parameters of the Lifshitz points in MnP and $Mn_{0.9}Co_{0.1}P$. The reduced scaling variables are $p=(T_L-T)/T_L$ and $t=(H_L-H)/H_L$.

Universal parameter	System	Range of reduced variable	Value and error	Reference
	MnP, $\mathbf{H}\|\|\mathbf{b}$	$0.02<p<0.31$	0.63 ± 0.03[a]	Ref. 11
	MnP, $\mathbf{H}\|\|\mathbf{b}$	$0.01<p<0.21$	0.605 ± 0.017	Ref. 13
Crossover	MnP, $\mathbf{H}\|\|\mathbf{b}$	$0.01<p<0.13$	0.596 ± 0.032	Ref. 32
exponent	MnP, $\mathbf{H}\perp\mathbf{c}$, 45° from b	See Ref. 17	0.61 ± 0.02	Ref. 17
ϕ	MnP, $\mathbf{H}\perp\mathbf{c}$, 25° from b	See Ref. 17	0.60 ± 0.02	Ref. 17
	MnP, $\mathbf{H}\|\|\mathbf{a}$	$0.02<p<0.34$	0.64 ± 0.02[a]	Ref. 8
	$Mn_{0.9}Co_{0.1}P$ $\mathbf{H}\|\|\mathbf{b}$	$0.03<p<0.25$	0.64 ± 0.04[a]	Ref. 16
Wave vector		$0.03<p<0.26$	0.44 ± 0.05[b]	Ref. 7
exponent	MnP, $\mathbf{H}\|\|\mathbf{b}$	$0.03<p<0.26$	0.49 ± 0.03[c]	Ref. 7
β_k		$0.03<p<1$	0.480 ± 0.013	Ref. 12
Magnetization jump exponent β_m	$Mn_{0.9}Co_{0.1}P$, $\mathbf{H}\|\|\mathbf{b}$	$0.04<p<0.2$	0.5 ± 0.05[d]	Ref. 16
Specific heat exponent α_L	MnP, $\mathbf{H}\|\|\mathbf{b}$	$0.004<t<0.2$	$0.4\div0.5$[e]	Ref. 14
Specific heat amplitude ratio of A^+/A^-	MnP, $\mathbf{H}\|\|\mathbf{b}$	$0.004<t<0.2$	0.65 ± 0.05	Ref. 14

[a]Final value comprising an estimate of the systematic error. The values and standard deviations for individual least-squares fits are given in the respective papers.
[b]The estimate from the neutron diffraction data alone.
[c]The estimate from the neutron diffraction data combined with the known location of the fan-para phase boundary at the phase diagram.
[d]See the remark given in Ref. 44.
[e]Value estimate under the assumption $\alpha^+=\alpha^-$. For other fit conditions see Ref. 14.

mental data for $Mn_{0.9}Co_{0.1}P$ (Ref. 16) show, however, that the hysteresis width of the ferro-fan transition is also described by the power law with an exponent close to the value of β_m.

The specific heat exponent α_L and corresponding amplitude ratio A^+/A^- are the only experimentally determined universal quantities which are concerned with a measurement along the t scaling axis.

B. Departure from the asymptotic critical behavior in the mean field theory

The power laws [Eqs. (15)–(19)] with classical exponents and amplitude ratios are obeyed by the present model in a close neighborhood of the LP. This provides numerical evidence that the used discrete spin model is consistent with the mean field solution for the relevant LGW Hamiltonian (with the order parameter varying continuously in space). However, the departure from asymptotic behavior is substantial for the model parameters κ and h corresponding to the range of temperatures T and magnetic fields H actually used in the experiments. The discrete spin model explains the origin of the departure from power laws and allows us to analyze this effect quantitatively.

Three reasons for the departure from asymptotic power laws seem most important. The first, which concerns the ordered phase only, is saturation of the order parameter. The order parameter for the LP in MnP is the magnetization component perpendicular to the applied field (i.e., m_y for $\mathbf{H}\|\mathbf{b}$), spatially uniform for the ferromagnetic phase and modulated for the fan phase. For the ferromagnetic phase it can be calculated as $m_y=\sqrt{1-(h/h_L)^2}$ and its value for $\kappa=-0.256$ (corresponding to $p=0.25$) at the F-FAN boundary is as large as 0.67. Saturation of the order parameter leads to the fact that the ferro-fan line becomes close to straight line at both experimental and calculated phase diagrams (for $\mathbf{H}\|\mathbf{b}$) for $T<80$ K whereas the critical fan-para line remains curved in the same temperature region.

The second effect is the nonlinear dependence between Hamiltonian parameters and physical variables. For the well-known example of a bicritical point in antiferromagnets the change of the effective anisotropy constant (appearing in the Hamiltonian) is proportional to the square of the applied magnetic field; hence respective fits of power laws to phase boundaries were made in T vs H^2 coordinates.[42] For the present model of MnP the relevant parameter κ is a nonlinear function of temperature because the slope of $\kappa(T)$ has to decrease gradually to zero at 0 K due to the third law of thermodynamics. [As modeled in this work by Eq. (14).]

The last source of limited applicability of Eqs. (16), (17), and (18), specific to multicritical points, is the direction of the weak scaling axis. The successful determination of the crossover exponent and the related amplitude ratio for bicritical points was possible because of use of an optimum scaling direction. The method to determine an optimum di-

rection of the ''weak'' scaling axis for the bicritical point from other experimental data was given by Fisher[42] using mean field arguments.

The same idea may be applied for the Lifshitz point in MnP. For the mean field solution of the LGW Hamiltonian the lines $q=\text{const}$ are parallel to the t axis. One of motivations for the present work was to apply the localized spin model to calculate the $q=\text{const}$ lines. If they are parallel straight lines, then their slope should provide the direction of the weak t axis. Figure 11 shows $q=\text{const}$ lines at the calculated phase diagram. Their slope depends on the distance to the LP and asymptotically ($p\rightarrow 0$) the direction of $q=\text{const}$ lines coincides with the vertical $\kappa=-1/4$ line. Thus, unfortunately, we cannot introduce a nonorthogonal scaling coordinate system but rather a nonlinear scaling coordinates.

The positive slope of the t scaling axis at $p=0$ is expected, for all ANNN-like models, as an effect of the critical fluctuations. The t axis is tangent to so-called disorder line[22,43] (in paramagnetic phase) which is curved due the shift of the LP coordinate κ_L to a value less than $-1/4$. The inclined direction of the t axis has been used in the recent work for the ANNNI model,[43] aiming at the estimation of some LP exponents using a high-temperature series expansion (HTSE) method. As emphasized by Mo and Ferrer ''our estimates are more reliable not only because we have longer series for a close-packed lattice but also primarily because we have analyzed our series along the appropriate scaling direction.''

C. Calculation of effective exponents

The deviation from asymptotic power laws is quantitatively described in this work by calculating the effective exponents. The concept of effective exponents is hardly elegant since they depend on the fit range and the conditions of the fitting procedure. They can, however, be directly compared to experimental exponents, because their calculation mimics the procedure of fitting the power law to experimental points in a finite range of temperature. Calculation of the effective exponents for different fit conditions reveals that the difference between exact results and the fitted power law with three free parameters is typically smaller than the corresponding experimental error in real data. This means that deviation from asymptotic behavior cannot be discerned in comparison to a real change of exponent (due to fluctuations) by the sole analysis of the fit quality.[44]

The effective exponents ϕ, β_k, and β_m shown in Fig. 12 were calculated by making a least-squares fit of the power laws, Eqs. (17)–(19), with $p=\kappa_L-\kappa$, to the calculated data points equally spaced between the given value of κ and the LP coordinate κ_L. The former was fixed at the value $\kappa_L=-1/4$.

Figure 12 also shows the effective amplitude ratio $F_1/F_{\lambda *}$ for the phase boundaries. It was calculated using the formula

$$F_1/F_{\lambda *}=\frac{h_L-h_{F\text{-}FAN}}{h_{FAN\text{-}P}-h_L}, \tag{20}$$

which makes it possible to define its effective value independently of the value of ϕ. The second amplitude ratio

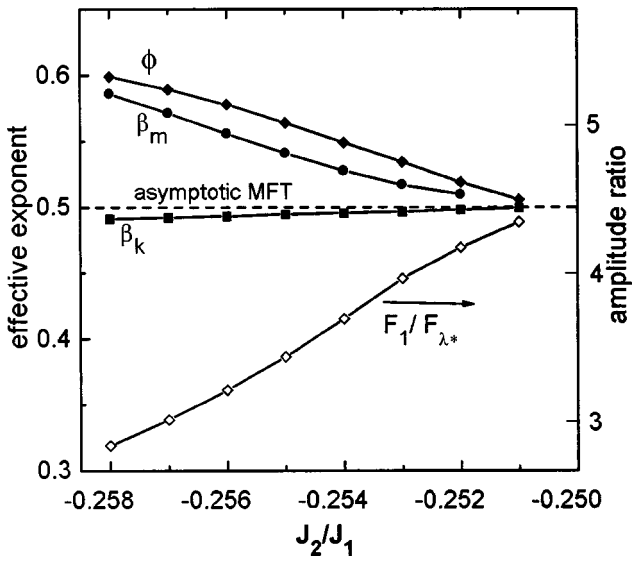

FIG. 12. Evolution of the effective exponents and amplitude ratio $F_1/F_{\lambda *}$ with the range of J_2/J_1.

$F_\lambda/F_{\lambda *}=0$ because the ferro-para phase boundary coincides with the p axis.

The deviation of effective exponents from mean field theory (MFT) values increases, in a nonlinear manner, with an increasing range of the p scaling variable. The sign and the value of this deviation are different for various universal parameters. For example, for the fit range $-0.258<\kappa<-1/4$, calculated effective values of ϕ, β_k, β_m, and $F_1/F_{\lambda *}$ deviate, respectively, $+20\%$, -2%, $+17\%$, and -36% off the asymptotic MFT values. This fit range, corresponding to $(T_L-T)/T_L=0.3$, is typical of many experiments (Table I).

These deviations become larger when the LP coordinate is a variable fitting parameter and/or the transformation of κ and h into the experimental variables T and H is used. Hence Fig. 12 shows the *lower limit* of the change in the effective exponent for a given fit range.

D. Discussion

Calculation of effective exponents shows that in an analysis of the experimental data the mean-field-type deviation from asymptotic power laws should be considered together with the real change of critical exponents due to critical fluctuations. In principle, both effects can be distinguished from each other by analyzing the dependence of the fitted exponent on the fit range. However, in many cases such a procedure cannot be successful due to the limited range of the experimental data (not much exceeding one decade of the reduced temperature) and their limited accuracy.

The value of the wave vector exponent in renormalization group calculations, $\beta_k=0.54$, shows only a small deviation from the MFT value of 1/2. This is because the difference arises only in the second order of the ϵ_L expansion.[45,46] The conclusion that β_k remains close to the classical value was confirmed more recently by HTSE calculations.[43] The accuracy of experiment of Moon, Cable, and Shapira[7] seems insufficient to discriminate between MFT and renormalization group (RG) values.

The present calculation explains, in fact, the values of β_k obtained in this experiment, which were found to be smaller

than 0.5. (See Table I.) On can calculate the value $\beta_k = 0.46$ by fitting the power law (17) with the variable T_L to the set of $q_{FAN\text{-}P}$ values calculated for the six temperatures used in the experiment.[7] Qualitatively, this decrease of the effective exponent is the combined effect of the nonlinearity of the $q^2(\kappa)$ function [Eq. (7)] and the nonlinear dependence of the competition ratio κ on the temperature [Eq. (14)].

For the crossover exponent the effect of critical fluctuations predicted by RG theory is substantial. The value $\phi = 0.625$, obtained using the first-order ϵ_L expansion,[47] was considered the natural explanation for experimental results. The present calculation reveals that, unfortunately, a similar change in the effective exponent (both sign and magnitude) results from classical deviation from asymptotic power laws. We think that the experimental values $\phi = 0.63-0.64$,[8,9,11,16] determined in a wide range of p (about 0.3), reflect rather a mean field correction to scaling. This is because the experimental determination of ϕ strongly relies on the shape of the ferro-fan phase boundary far away from the LP. This first-order line in the corresponding temperature range is unlikely to be influenced by critical fluctuations and is affected by all discussed MFT-type corrections to scaling.

Experiments of the Sao Paulo group[13,15,17] bring actually the best data for determination of the crossover exponent. The measurements of the ac susceptibility (both in phase χ' and out-of-phase χ'' components) were made using a spherical sample, the same for which the determination of the exponent α_L was made.[14] The data points for ferro-fan and fan-para transitions were resolved for $T_L - T$ as small as 1 K ($p = 0.01$), thus allowing to make fits in a closer neighborhood of the LP. The rapid variation of the χ'' peak amplitude along the critical boundary provides the location of the LP independent of the fit to the phase boundaries. The values of ϕ for $p < 0.21$ and $p < 0.13$ quoted in Table I suggest that the asymptotic value of the crossover exponent is lower than 0.6. (This conclusion is supported by the explicitly calculated dependence of ϕ on the fit range given in Table I of Ref. 17.) The question remains as to whether this asymptotic value remains higher (beyond the limit of error) than the classical value 1/2.

For the present model the amplitude ratio $F_\lambda / F_{\lambda *}$ is zero and this conclusion is consistent with experiment. The experimental value of this universal quantity is, in our opinion, in qualitative disagreement with the value -1 provided by RG theory.[47]

For both the crossover exponent ϕ and amplitude ratio $F_\lambda / F_{\lambda *}$ the available theoretical values from RG theory are quite uncertain. Both are known only to the first-order ϵ_L expansion which is more inaccurate than the standard ϵ expansion because $\epsilon_L = 3/2$ for the three-dimensional uniaxial LP. An alternative value for the crossover exponent can be obtained from the scaling laws[45] $\phi = \nu_{L4}/\beta_k$ and $\phi = \nu_{L4}(2 - \eta_{L4} - \lambda)$, as a combination of the relatively accurate HTSE value[43] $4\nu_{L4} = 1.63 \pm 0.10$ and the remaining exponents known in the second-order ϵ_L expansion. The thus obtained estimates of ϕ are above 0.7, hence even more difficult to reconcile with the asymptotic experimental value which seems to be lower than 0.6.

No prediction beyond MFT is available for the magnetization jump exponent β_m and the amplitude ratio $F_1 / F_{\lambda *}$. The present calculation explains the dependence $\Delta M(T)$ obtained for $Mn_{0.9}Co_{0.1}P$.[16,44]

For the $F_1 / F_{\lambda *}$ amplitude ratio the departure from the asymptotic value is negative and the largest of all calculated universal parameters. Calculation shows that the effective $F_1 / F_{\lambda *}$ strongly depends on the direction of the t axis. An inspection of Fig. 11 shows that when one uses the inclined t axis with a slope consistent with $q = \text{const}$ lines one obtains $F_1 / F_{\lambda *}$ values which are more close, but actually higher, than the asymptotic MFT value 4.45.

The overview of universal parameters related to the p scaling variable shows that their experimental values seem consistent with mean field theory (with a possible exception for ϕ). We do not know whether they are really in conflict with modern theories of critical phenomena because no estimation for the range of the Lifshitz-type critical behavior along the p axis was made.

The conclusion that the actually known universal parameters related to the p scaling variable are consistent with classical theory is not easy to understand also because there are indications that critical fluctuations are active in MnP. The critical behavior with nonclassical values of β and γ exponents was found around the Curie point $T_C = 291$ K in a rather wide range of temperatures and fields.[48] The observation of Bindilatti and co-workers[13–15] of the λ-shaped divergence of the longitual susceptibility in the vicinity the Lifshitz point, making possible a determination of the α_L exponent, remains qualitative evidence of the nonclassical nature of the LP in MnP. (The present MFT calculation predicts a finite jump of the magnetic susceptibility $\chi = dm/dh$ corresponding to $\alpha_L = 0$.)

Manganese phosphide remains the best example of the Lifshitz point in a real physical system and may deliver new relevant experimental data. The measurements of β_L and γ_L exponents seems important because their RG and HTSE values[22,43] are very different when compared to the MFT values. The crucial experiment in ascertaining the nature of the Lifshitz point in MnP should be an investigation of critical fluctuations.[49,50]

VI. CONCLUSIONS

The zero-temperature solution for a simple localized spin model explains a set of experimental results of incommensurate phases of MnP for which a quantitative theory or even qualitative interpretation was lacking. They include the bunching of moments in the helimagnetic phase, the field dependence of the modulation vector in all three modulated phases, and the shape of their magnetization curves. The calculated magnetic phase diagrams for the three principal directions of applied field remain in semiquantitative agreement with experiment.

For the Lifshitz point occurring at a confluence of fan, ferromagnetic, and paramagnetic phases the localized spin model allowed us to calculate the effective (fit-range-dependent) values for the crossover exponent ϕ, propagation vector exponent β_k, magnetization jump exponent β_m, and two amplitude ratios for phase boundaries. Model results concerning the Lifshitz point were thoroughly discussed in Sec. V D. In general they indicate that to understand the experimental values of these universal LP parameters the mean field corrections to scaling should be taken into ac-

count together with the results of the fluctuational theories.

The model predictions which are to be tested experimentally comprise the field dependence of the wave vector in the cone and fan phases for **H**∥**a**, and the weakly-first-order nature of the cone-fan transition.

The present calculations are limited to an external field applied along the three principal orthorhombic directions. The zero-temperature solution can also be obtained for an arbitrary direction of the applied field.[51] The resulting topology of suitable many-dimensional magnetic phase diagram contains the line of Lifshitz points for the direction of magnetic field within the *ab* plane (confirmed experimentally by Becerra, Brumatto, and Oliveira[17]) and the line of tricritical points for *H* within the *bc* plane (discussed by Shapira *et al.*[11]).

The results of the simplest zero-temperature solution give us confidence that the ANNNH model with estimated values of the model parameters describes the essential physics of the magnetic phases and phase transitions of MnP. This Hamiltonian seems simple enough to make practical calculations beyond MFT using theoretical methods (like HTSE or Monte Carlo) which are capable of bringing information on the nonuniversal effects of critical fluctuations. Different phenomena induced by quenched disorder, observed in $Mn_{0.9}Co_{0.1}P$, also await for a theoretical interpretation.[52]

ACKNOWLEDGMENTS

The authors thank J. Jensen and Y. Shapira for a critical reading of the manuscript.

APPENDIX: ENERGY FOR DIFFERENT SPIN CONFIGURATIONS

The symbols appearing in Eqs. (A1)–(A8) are defined in Sec. II.

Helimagnetic phase:

$$e(q)=-\frac{j(q)}{2}+\frac{k}{2}-\frac{k^2}{2[j(q)-j(3q)]}-\frac{h^2}{2[2j(q)-j(2q)-j(0)\pm 2k]}\left[1\pm\frac{2k}{j(q)-j(3q)}\right]. \tag{A1}$$

The signs + and − in the symbol ± correspond to **H**∥**b** and **H**∥**c**, respectively.

Fan phase (**H**∥**b**):

$$e(q)=-\frac{j(0)}{2}+k-h-\frac{[j(q)-j(0)+2k-2h]^2}{3j(q)-j(2q)-2j(0)+6k}. \tag{A2}$$

For **H**∥**c** and **H**∥**a** the anisotropy parameter k in Eq. (A2) should be replaced by $-k$ and k^z, respectively.

Elliptical cone (**H**∥**a**): The fourth-order power expansion for the energy is given by

$$e(\xi,\zeta,q)=c+b_1\xi^2+b_2\zeta^2+a_1\xi^4+a_2\zeta^4+2d\xi^2\zeta^2, \tag{A3}$$

with coefficients

$$c=-\frac{j(0)}{2}+k^z-h,$$

$$b_1=\tfrac{1}{4}[j(0)-j(q)-2k^z+h],\quad b_2=b_1-\tfrac{1}{2}k,$$

$$a_1=\tfrac{1}{64}[-2j(0)+3j(q)-j(2q)+6k^z],\quad a_2=a_1+\tfrac{3}{32}k,$$

$$d=\frac{1}{64}[-j(0)+j(2q)+h]. \tag{A4}$$

The energy minimized with respect to ξ and ζ reads

$$e(q)=c-\frac{1}{4}\frac{a_1b_2^2+a_2b_1^2-2db_1b_2}{a_1a_2-d^2}. \tag{A5}$$

Circular cone (**H**∥**a**):

$$e(q)=-\frac{1}{2}\left[j(q)+k+\frac{k^2}{j(q)-j(3q)}-\frac{h^2}{2j(q)-j(2q)-j(0)+2k}\right]. \tag{A6}$$

Ferromagnetic phase (**H**∥**b**):

$$e=-\frac{j(0)}{2}-\frac{h}{4k}. \tag{A7}$$

For **H**∥**a** the anisotropy parameter k should be replaced by k^z.

Paramagnetic phase (**H**∥**b**):

$$e=-\frac{j(0)}{2}+k-h. \tag{A8}$$

For the **H**∥**c** and **H**∥**a** cases k should be replaced by 0 and k^z, respectively.

[1] E. E. Huber and D. H. Ridgley, Phys. Rev. **135**, A1033 (1964).
[2] R. M. Moon, J. Appl. Phys. **53**, 1956 (1982).
[3] T. Komatsubara, K. Kinoshita, and E. Hirahara, J. Phys. Soc. Jpn. **20**, 2036 (1965).
[4] Y. Ishikawa, T. Komatsubara, and E. Hirahara, Phys. Rev. Lett. **23**, 532 (1969).
[5] H. Obara, Y. Endoh, Y. Ishikawa, and T. Komatsubara, J. Phys. Soc. Jpn. **49**, 928 (1980).
[6] H. Fjellvag and A. Kjekshus, Acta Chem. Scand. **38**, 563 (1984).
[7] R. M. Moon, J. W. Cable, and Y. Shapira, J. Appl. Phys. **52**, 2025

(1981).
[8] Y. Shapira, N. F. Oliveira, Jr., C. C. Becerra, and S. Foner, Phys. Rev. B **29**, 361 (1984).
[9] C. C. Becerra, Y. Shapira, N. F. Oliveira, Jr., and T. S. Chang, Phys. Rev. Lett. **44**, 1692 (1980).
[10] M. C. Barbosa, Physica B **215**, 286 (1995).
[11] Y. Shapira, C. C. Becerra, N. F. Oliveira, Jr., and T. S. Chang, Phys. Rev. B **24**, 2780 (1981).
[12] Y. Shapira, in *Multicritical Phenomena*, edited by R. Pynn and A. Skjeltorp, Vol. 106 of *NATO Advanced Study Institute, Series B: Physics* (Plenum, New York, 1984), p. 53.
[13] V. Bindilatti, Ph.D. thesis, University of Sao Paulo, 1988 (in Portuguese).
[14] V. Bindilatti, C. C. Becerra, and N. F. Oliveira, Jr., Phys. Rev. B **40**, 9412 (1989).
[15] C. C. Becerra, V. Bindilatti, and N. F. Oliveira, Jr., in *New Trends in Magnetism*, edited by M. D. Coutinho-Filho and S. Rezende (World Scientific, Singapore, 1990).
[16] A. Zieba, C. C. Becerra, H. Fjellvag, N. F. Oliveira, Jr., and A. Kjekshus, Phys. Rev. B **46**, 3380 (1992).
[17] C. C. Becerra, H. J. Brumatto, and N. F. Oliveira, Jr., Phys. Rev. B **54**, 15 997 (1996).
[18] C. C. Becerra, N. F. Oliveira, Jr., and A. C. Migliano, J. Appl. Phys. **63**, 3092 (1989).
[19] C. C. Becerra, A. Zieba, N. F. Oliveira, Jr., and H. Fjellvag, J. Appl. Phys. **67**, 5442 (1990).
[20] A. Zieba, C. C. Becerra, N. F. Oliveira, Jr., H. Fjellvag, and A. Kjekshus, J. Magn. Magn. Mater. **104-107**, 71 (1992).
[21] R. M. Hornreich, M. Luban, and S. Shtrikman, Phys. Rev. Lett. **35**, 1678 (1975).
[22] For a recent review, see W. Selke, in *Phase Transitions and Critical Phenomena*, edited by C. Domb and J. Lebowitz (Academic, London, 1992), Vol. 15.
[23] T. Nagamiya, K. Nagata, and Y. Kitano, Prog. Theor. Phys. **27**, 1253 (1962).
[24] Y. Kitano and T. Nagamiya, Prog. Theor. Phys. **31**, 1 (1964).
[25] K. Inomata and T. Oguchi, J. Phys. Soc. Jpn. **25**, 1533 (1968).
[26] S. Hyamitzu and T. Nagamiya, Int. J. Magn. **2**, 33 (1972).
[27] J. Smit, Solid State Commun. **47**, 87 (1983).
[28] C. S. O. Yokoi, M. D. Coutinho-Filho, and S. R. Salinas, Phys. Rev. B **24**, 5430 (1981).
[29] J. L. Cadorin and C. S. O. Yokoi, Phys. Rev. B **56**, 11 635 (1997).
[30] C. C. Becerra, N. F. Oliveira, and Y. Shapira, J. Phys. (Paris), Colloq. **8**, C12-895 (1988).
[31] J. Jensen, Phys. Rev. B **54**, 4021 (1996), and references therein.
[32] L. Dobrzynski and A. F. Andresen, J. Magn. Magn. Mater. **82**, 67 (1989).
[33] K. Tajima, Y. Ishikawa, and H. Obara, J. Magn. Magn. Mater. **15-18**, 373 (1980).
[34] H. Yoshizawa, S. M. Shapiro, and T. Komatsubara, J. Phys. Soc. Jpn. **54**, 3084 (1985).
[35] Due to the different notation, the Hamiltonian parameters J_1, K, and K^z in this work should be compared, respectively, to $2J_1$, $2D_2$, and D_1+D_2 in Ref. 34.
[36] See Eq. (3.7) in Ref. 25. Its denominator should be multiplied by 2.
[37] C. C. Becerra (private communication).
[38] E. Rastelli and A. Tassi, J. Appl. Phys. **69**, 5798 (1991).
[39] For experimental data, see A. Takase and T. Kasuya, J. Phys. Soc. Jpn. **47**, 491 (1979). They fit their data using a more complex two-parameter formula, but we use the ''3/2 law'' as the simplest one-parameter approximation.
[40] N. F. Oliveira, Jr., A. Paduan-Filho, S. R. Salinas, and C. C. Becerra, Phys. Rev. B **18**, 6165 (1978).
[41] C. C. Becerra, N. F. Oliveira, Jr., A. Paduan-Filho, W. Figueiredo, and M. V. P. Souza, Phys. Rev. B **38**, 6887 (1988).
[42] M. E. Fisher, Phys. Rev. Lett. **34**, 1634 (1975).
[43] Z. Mo and M. Ferer, Phys. Rev. B **43**, 10 890 (1991).
[44] The deviation from the asymptotic power law for the magnetization discontinuity along the ferro-fan line is qualitatively evidenced by the convex shape of the ΔM^2 vs T curve in Fig. 8 in Ref. 16. All experimental points in this graph ($t>0.33$) can well be fitted by the three-parameter power law with $\beta_m=0.67(2)$. The former result was not accepted (and not given in Ref. 16) because the value $T_L=94.8(4)$ K obtained from such a fit is incompatible with $T_L=99$ K determined from the fit to phase boundaries. It was stated instead that the experimental points are consistent with the value $\beta_m=1/2$ in the limited range of reduced temperature ($t<0.2$).
[45] D. Mukamel, J. Phys. A **10**, L249 (1977).
[46] R. M. Hornreich and A. Bruce, J. Phys. A **11**, 595 (1978).
[47] D. Mukamel and M. Luban, Phys. Rev. B **18**, 3631 (1978).
[48] H. Terui, T. Komatsubara, and E. Hirahara, J. Phys. Soc. Jpn. **38**, 383 (1975).
[49] The authors of Ref. 34 state, on p. 3085, ''We also observed that the quasielastic scattering near the LP does show the q^{-4} dependence.''
[50] ''I definitely saw quasielastic scattering at or near the LP of the form $A/(B+Cq^4)$.'' R. P. Moon (private communication).
[51] For a field confined to the easy *bc* plane the relevant formulas are given in Ref. 26.
[52] An example of such a theory (not directly related to $Mn_{0.9}Co_{0.1}P$) is a MF calculation for the ANNNI model in a random field by M. N. Tamashiro, C. S. O. Yokoi, and S. R. Salinas, Phys. Rev. B **56**, 8204 (1997).